

RNN-Based GNSS Positioning using Satellite Measurement Features and Pseudorange Residuals

Ibrahim Sbeity^{*†}, Christophe Villien^{*}, Benoît Denis^{*}, and E. Veronica Belmega^{‡†}

^{*} CEA-Leti, Université Grenoble Alpes, F-38000 Grenoble, France

[†] ETIS UMR 8051, CY Cergy Paris Université, ENSEA, CNRS, F-95000, Cergy, France

[‡] Univ. Gustave Eiffel, CNRS, LIGM, F-77454, Marne-la-Vallée, France

Emails: ibrahim.sbeity@cea.fr, christophe.villien@cea.fr

Abstract—In the Global Navigation Satellite System (GNSS) context, the growing number of available satellites has led to many challenges when it comes to choosing the most accurate pseudorange contributions, given the strong impact of biased measurements on positioning accuracy, particularly in single-epoch scenarios. This work leverages the potential of machine learning in predicting link-wise measurement quality factors and, hence, optimize measurement weighting. For this purpose, we use a customized matrix composed of heterogeneous features such as conditional pseudorange residuals and per-link satellite metrics (e.g., carrier-to-noise power density ratio and its empirical statistics, satellite elevation, carrier phase lock time). This matrix is then fed as an input to a recurrent neural network (RNN) (i.e., a long-short term memory (LSTM) network). Our experimental results on real data, obtained from extensive field measurements, demonstrate the high potential of our proposed solution being able to outperform traditional measurements weighting and selection strategies from state-of-the-art.

Index Terms—Satellite Selection, Single-epoch Positioning, Machine (Deep) Learning, Long-Short Term Memory Neural Network, Satellite Measurement Features

I. INTRODUCTION

Accurate outdoor positioning using Global Navigation Satellite System (GNSS) is a key enabler for many important applications, such as autonomous vehicles and unmanned aerial vehicles, tracking of blue force and first responders, seamless end-to-end logistics and supply chains optimization, large-scale crowd sensing, etc. To ensure reliable positioning, several satellite vehicle (SV) selection, fault detection and exclusion (FDE), and weighting techniques, must be performed during the tracking phase of the navigation processor. However, in a single-epoch context, the problem becomes even more challenging, taking into consideration that there is no access to prior estimates.

Despite these challenges, single-epoch positioning remains essential in several operating contexts. First, it can serve as an initial position estimate to initialize the navigation processor [1]. Second, the loosely-coupled data fusion of GNSS with an Inertial Navigation System (INS) requires the GNSS outputs (i.e., position and velocity) to be independent. This is to prevent any time-correlated measurements from occurring at the input of the fusion engine. Therefore, single-epoch solutions are necessary. Finally, recently developed Internet of Things (IoT) chips, such as Semtech’s LoRa chip LR1110 [2], utilize

low-power receivers to capture a single snapshot of GNSS measurements. These measurements are then transmitted via the IoT network to undergo remote cloud processing. Despite the imposed single-epoch framework, the processing power is not actually limited.

In this context, the signals received from satellites in harsh environments such as urban canyons can be significantly impacted by Non-Line of Sight (NLOS) and multi-path (MP) propagation, resulting in strongly biased pseudorange measurements. It is hence crucial to identify the most reliable and informative measurements while disregarding the most harmful ones. This selection process is especially challenging as modern GNSS receivers typically receive tens of measurements from different constellations at each time epoch. Basic selection approaches primarily rely on single-link satellite features, such as the signal carrier-to-noise power density ratio (C/N_0) or the elevation angle (θ), to exclude or mitigate the impact of satellites that are likely to contribute to large positioning errors [3], [4].

Several techniques have been proposed to select the remaining satellites that meet basic single-link quality criteria, including subset-testing [5], RANdom SAMple Consensus (RANSAC) [6], iterative reweighting [7], etc. These methods offer various trade-off levels between computational complexity and performance. However, because of the massive combinatorial complexity of testing all possible subsets of satellites, exhaustive search is not feasible and the selection problem remains an open issue to the best of our knowledge. Conventional selection approaches [8], rely on the spatial distribution of intermediate positioning results conditioned on specific satellite subsets to determine the most harmful contributions. These approaches only exclude satellites with strongly biased pseudoranges instead of mitigating for these biases. This may limit the best possible positioning accuracy accordingly.

In this paper, we present a new pre-processing approach specifically designed for single-epoch stand-alone positioning, which addresses the limitations of conventional satellites selection techniques. Our approach casts the initial satellite selection problem into a weighting problem. A first innovative aspect lies in exploiting machine learning (ML) into the domain of pseudorange residuals, resulting from offline condi-

tional positioning results, jointly with that of instantaneous SV measurements, such as C/N_0 and angle elevation, to optimize satellite weights.

To fully exploit the potential of deep learning tools in uncovering the hidden correlations between pseudorange measurements and the position solution, as well as possible joint effects of discarding multiple measurements at a time, we exploit a long-short term memory neural network (LSTM NN) from the family of recurrent neural networks (RNNs) that is fed with a customized feature matrix, what represents another originality of our contribution. The LSTM NN predicts quality factors that estimate the link-wise standard deviations of pseudorange errors. These predictions are then used to compute nearly-optimal satellite weights within a conventional weighted least squares (WLS) positioning solver.

The training and testing of our neural network (NN) were performed using real data collected from extensive field tests comprising more than 290 experiments (i.e., driving sessions) and 440,000 epochs. For this purpose, we used a receiver capable of operating over multiple constellations in both single-band and dual-band modes. The ground-truth reference positioning data was collected from a high-end GNSS-aided INS system providing cm-level accuracy.

In summary, the main contributions of this paper are: First, we propose a novel deep learning-based solution to the satellite selection problem. Our approach relies on a LSTM NN fed with a customized matrix containing joint features (i.e., conditional pseudorange residuals) and per-link features (e.g., carrier-to-noise power density ratio and its statistics, elevation angle, carrier phase lock time). Second, our approach is shown to enhance the computation of measurement weights compared to conventional parametric methods. This has been verified through real-field data obtained by measurement campaigns and a dedicated test platform in various driving scenarios and environments.

II. PROBLEM FORMULATION

A. Single Epoch Positioning

To simplify the presentation and notations, with no loss of generality regarding the proposed approach, we consider here a set of N single band, single constellation, pseudorange measurements $\{\rho^i\}_{i=1\dots N}$. While accounting for experimental results in Section IV, we will consider a multi-band and multi-constellation scenario. The necessary corrections, computed from ephemeris data (such as SV clock bias, ionospheric and tropospheric delays, Sagnac correction, etc.), have already been applied to these pseudorange measurements. The measurement from the i -th SV, in the absence of MP or any strong bias, can be modeled as follows:

$$\rho^i = \sqrt{(x - x^i)^2 + (y - y^i)^2 + (z - z^i)^2} + c \delta + \eta^i, \quad (1)$$

where ρ^i is the pseudorange between the receiver and the i -th SV, with (x^i, y^i, z^i) and (x, y, z) the coordinates of the i -th satellite and the receiver, respectively. The parameter c is the speed of light, and δ is the clock bias between the receiver and the considered constellation. η^i is the observation

noise, which represents both the receiver noise and errors resulting from troposphere and ionosphere extra delays, etc. Although ionosphere and troposphere residual errors (i.e., after correction from navigation message) are highly correlated over time, they are usually considered as independent and zero mean in single-epoch processing. Hence, we simply assume that the observation noise follows a centered Gaussian distribution $\eta^i \sim \mathcal{N}(0, (\sigma^2)^i)$.

Our aim is to estimate the vector $\mathbf{X} = [x, y, z, \delta]^\top$ from the set of measurements $\{\rho^i\}_{i=1\dots N}$. A solution that is efficient and widely used is then provided by the maximum-likelihood estimator (MLE) [9], which simplifies to a WLS estimator for our Gaussian noise model:

$$\hat{\mathbf{X}} = \arg \min_{\mathbf{X}} \sum_{i=1}^N \omega^i (\rho^i - h^i(\mathbf{X}))^2, \quad (2)$$

where the observation function for the i -th satellite is defined as

$$h^i(\mathbf{X}) = \sqrt{(x - x^i)^2 + (y - y^i)^2 + (z - z^i)^2} + c \delta, \quad (3)$$

and the optimal weights are equal to

$$\omega^i = \frac{1}{(\sigma^2)^i}. \quad (4)$$

The solution can be computed using an optimization algorithm such as Levenberg-Marquardt or Gauss-Newton [10].

B. GNSS Satellite Selection and Weighting Problems

Generally, an initial rough SV selection based on satellite elevation or C/N_0 thresholds is performed to exclude presumably strongly biased measurements. Then, the standard deviation of the remaining measurements is estimated using an empirical function, for instance as follows [11]:

$$(\sigma^2)^i = \frac{1}{\sin^2(\theta^i)} \left(\sigma_{\rho Z}^2 + \frac{\sigma_{\rho c}^2}{(C/N_0)^i} + \sigma_{\rho a}^2 (a^2)^i \right), \quad (5)$$

This function mainly depends on satellite elevation θ , C/N_0 , acceleration a , and other empirically calibrated coefficients $(\sigma_{\rho Z}^2, \sigma_{\rho c}^2, \sigma_{\rho a}^2)$ that are hard to be fine-tuned.

However, some measurements could be strongly biased by MP for instance, and violate the expected Gaussian model, resulting in a significant degradation of the solution accuracy. It is thus of primary importance to exclude these measurements from the solution, either by discarding them or by assigning them a zero weight, which is also called de-weighting. Such measurements can be efficiently detected at the navigation processor stage based on innovation monitoring tests for instance [12], but this requires the tracking filter to have already converged and the predicted state (i.e., position, receiver clock offset, etc.) to be accurate enough.

For single epoch processing, no predicted solution is available and SV selection relies on measurements only with very limited prior knowledge. This implies that the detection of k faults among N measurements could potentially result in a huge number of subsets, C_k^N , to test in case of an exhaustive search, which is intractable in real-time and even for post-processing. As an example, assuming at most 10 faults among

40 measurements would result in more than 847×10^6 subsets to test, which is computationally prohibitive.

C. Existing Works

In the field of GNSS, improving the integrity of navigation solutions requires the identification and rejection of corrupt signals. FDE techniques, such as classical FDE [13], [14], advanced receiver autonomous integrity monitoring (ARAIM) [15], [16], brute force subset testing [17], and range consensus (RANCO) [8], have been proposed in the literature. Recently, a new FDE algorithm [18] has been put forward that utilizes both a standalone FDE block based on a residual test using WLS and an FDE-based Extended Kalman Filter (EKF). The algorithm alternates between the two branches depending on a covariance matrix threshold. When the covariance matrix falls below a pre-defined threshold, the EKF utilizing FDE is employed; otherwise, the FDE is used on its own. This algorithm has shown significant improvements in accuracy compared to conventional state-of-the-art FDE algorithms, and is hence used as a reference for benchmark purposes in this paper. However, since the focus is on single-epoch localization applications, only the standalone FDE block is utilized in this study.

III. PROPOSED SYSTEM ARCHITECTURE

As previously mentioned, we focus on single-epoch standalone positioning based on pseudoranges without differential corrections, where measurements have just been pre-processed (see Section II-A). Our main objective is to exploit the complex inter-dependencies and joint effects across multiple links using supervised deep learning. This will allow us to efficiently weight the contributions from all satellites.

For this, we first need to build a comprehensive set of information inputs to our NN. One novelty of our proposal is to concatenate both per-link and joint features, which will be detailed below, and feed them as one single customized matrix into the RNN (i.e., LSTM NN). The network is then trained to predict the weights $\hat{\omega}^i$ related to the underlying distribution of pseudorange errors according to (4). We expect our network to predict nearly null weights $\hat{\omega}^i \approx 0$ for strongly biased satellites to be excluded.

To sum up, the original difficult selection problem is cast into a soft weighting problem. Fig. 1 shows the complete architecture of our proposed solution.

A. Per-link Features

Several per-link measurement features can be informative, and hence beneficial to be provided as an input to the NN, such as: the SV elevation angle θ , the carrier phase lock time, C/N_0 and its empirical statistics (i.e., empirical variance σ_{C/N_0}^2 and mean $\overline{C/N_0}$ computed for the sliding window).

The intuition behind the SV elevation angle as a feature is based on the fact that signals from SV with low elevation angles have a longer traveling distance in the ionospheric and tropospheric layers and a greater probability of NLOS conditions. Also, the carrier phase lock time is an important indicator for newly acquired SVs.

Regarding C/N_0 , low values increase the tracking noise of the ranging processor and, consequently, increase the pseudorange measurement noise. Beyond, the statistics of C/N_0 (i.e., its variance and mean) are also expected to convey informative indications about the operating conditions. For instance, it has been observed that the short-term empirical variance, computed over a short period of time, could be a fairly good indicator of MP [19]. Even though we deal with single-epoch processing in our case, we can still practically approximate the actual variance of C/N_0 over a few past seconds, as it will only affect measurement weights and introduce minimal correlation between them.

For this purpose, we consider a sliding window to calculate both the empirical variance σ_{C/N_0}^2 and mean $\overline{(C/N_0)^i}$ of C/N_0 . This time window varies in size and contains the C/N_0 values from the previous epochs. As illustrated in Fig. 2, the size of the window is determined by the number of epochs in which a particular satellite was received, and it can reach a maximum of 10 epochs (equivalent to 2 seconds). If the window contains only one entry, the variance is set to an arbitrarily large value. At last, the size of the sliding window is also fed as a feature to the NN.

As a result, the obtained per-link features are concatenated into a sub-matrix containing 6 feature column vectors of dimension N (see Fig. 1).

B. Joint Features

Joint features accounting for the simultaneous impact of multiple measurements over distinct links (i.e., in contrast to per-link features) can also be extracted from the comparison of the positioning solutions from different tested subsets. To overcome the challenge of testing all the possible subset combinations, which is computationally prohibited, our approach leverages the ability of ML in extracting hidden inter-dependencies from only N such subsets.

At each navigation epoch, we assume that multiple (i.e., N) satellite signals are received and a new matrix of positioning residuals \mathbf{M} is constructed, as follows. We generate N subsets S_n of $N - 1$ satellites, where we exclude one distinct satellite (i.e., n^{th} satellite) at a time.

$$S_n = \{\rho^i\}, i = 1 \dots N, i \neq n \quad (6)$$

For each subset S_n , we calculate the corresponding solution X_n using (2) with equal weights. Then, for each of the N resulting positions $\{\mathbf{X}_1, \dots, \mathbf{X}_N\}$ we calculate the $N - 1$ pseudorange residuals

$$\delta \rho_{X_n}^i = \rho^i - h^i(\mathbf{X}_n), i \neq n \quad (7)$$

The coefficient $[\mathbf{M}]_{n,i}$ (i.e. row n , column i) of the residual matrix \mathbf{M} is then simply given by the corresponding residual for non-diagonal coefficients, or by an arbitrary large value γ for the diagonal terms, indicating that the satellite has been deliberately excluded.

$$[\mathbf{M}]_{n,i} = \begin{cases} \delta \rho_{X_n}^i, & i \neq n \\ \gamma, & i = n \end{cases} \quad (8)$$

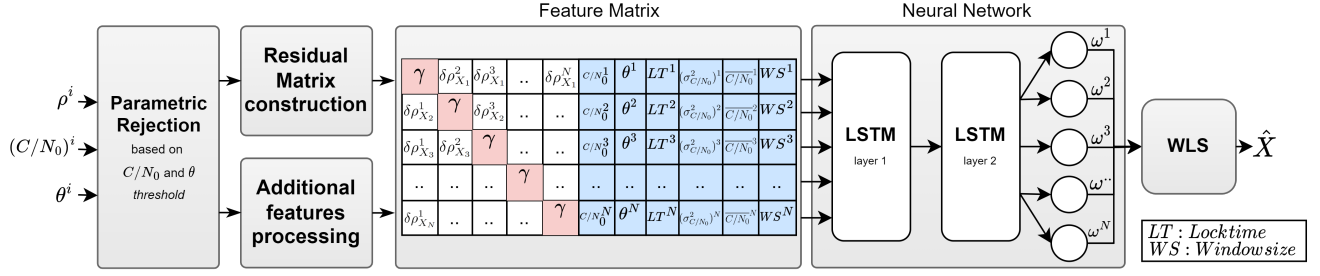


Fig. 1. Complete architecture of our proposed approach.

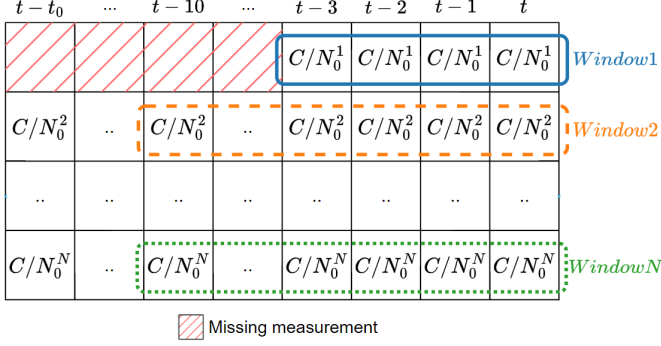


Fig. 2. Variable size sliding window for C/N_0 variance and mean calculation.

Each row n of the matrix will thus provide residuals associated with the exclusion of the n -th measurement. Although it assumes a single fault per subset (i.e., row), our intuition is that such a matrix is able to reveal the complex joint contributions of each satellite onto the positioning solution, while being fed as a single input to the NN.

C. Long-Short Term Memory Neural Network

The overall input matrix of features being fed to the NN can be seen as a sequence of N pseudo-observations. At each observation, a single pseudorange measurement is excluded from computing the solution. By analyzing this sequence, the LSTM NN can exploit the correlations between the excluded measurement and the solution and pinpoint which measurement exclusions have the best impact on the quality of the positioning solution. As a result, the NN will be capable of predicting weights that exclude multiple biased measurements by analyzing the sequence of pseudo-observations, set as joint features (see Section III-B). Besides, the additional per-link features for the excluded measurements were concatenated for each pseudo-observation to provide more information about the excluded satellites (see Section III-A).

In this kind of problems, the LSTM NN architecture, which is a type of RNN [20], has the advantage of keeping memory over multiple (possibly distant) pseudo time steps. Hence, it is also suited to exploit the correlations across the matrix rows in our case, even if we explicitly deal with a single-epoch problem. Similar applications of the LSTM NN to other time-invariant problems have already been considered. For instance, in [21], LSTM NN was used to process data with long-range interdependence (i.e., using geometric properties of the trajectory for unconstrained handwriting recognition).

Note that several other (more complex) NN architectures were evaluated. For instance, we considered a more complex architecture composed of two different concatenated NNs. The first NN processes only the residual matrix as input. Its output is concatenated with the additional per-link features and fed as inputs to the second fully-connected NN (FCNN). However, such architectures did not provide any significant improvement over the LSTM NN that only processes the residual matrix. For the sake of conciseness, such alternative architectures are not further discussed in this paper.

IV. NUMERICAL RESULTS

To assess both the feasibility of our approach and the impact of using a customized residual matrix to capture interdependencies between the measurements and the computed solution, we conducted two tests. First, we evaluated our approach using only the residual matrix as input to the NN. Second, we evaluated our approach using the overall feature matrix (containing the residuals coupled with the per-link features) as an input. The results obtained were compared with the state-of-the-art (SOTA) approach [18] described in Section II-C.

A. Data Collection and Scenarios

We conducted our tests on real-world data collected from measurement campaigns under various operational conditions. These conditions included open skies, dense urban areas, and a range of mobility scenarios. The data was collected using Vehloc, a multi-sensor platform developed by CEA-Leti. This board can be equipped with one out of two different receiver chips: either a NEO-M8P or a ZED-F9P, both from Ublox. The ZED-F9P dualband RTK GNSS chip can receive up to $N = 60$ satellite signals from various GNSS constellations (including GALILEO, GPS, GLONASS, etc.) across multiple frequencies (i.e., L1, L2, E1, and E5 bands). The NEO-M8P chip can receive single-band L1 signals from multi-constellation (i.e., only GPS and GLONASS were used).

The raw measurements were collected at a rate of 5 Hz, as well as the broadcasted ephemeris. These measurements included the SV ID, constellation ID, frequency ID, pseudorange, pseudorange rate, carrier phase, C/N_0 , carrier phase lock time, etc. The reference position was obtained from a high-end, GNSS-aided INS, Ekinox platform from SBG, which was post-processed using Qinertia software (from SBG) to provide centimeter-level accuracy, even in difficult GNSS conditions. The complete experimental setup is depicted in

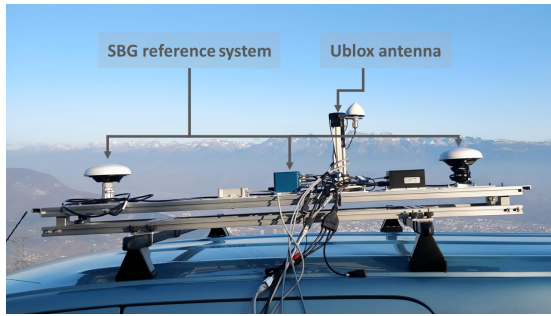


Fig. 3. Data collection setup.

Fig. 3, which shows the Ublox antenna of the Vehloc platform and the SBG reference system mounted on the roof of a vehicle. In total, 291 experiments were conducted during the data collection campaigns phase, which yielded a diverse, representative, and comprehensive dataset for evaluation, encompassing up to 440,000 epochs.

B. Evaluation Results

The architecture of our NN including the number of layers and the number of neurons per layer was optimized empirically. So as to prevent overfitting effects, an early stopping callback was used during the training process. Data was randomly split into three disjoint subsets: 60% of the data for training, 20% of the data for validation, and 20% for testing and evaluating the performance of our approach (i.e., unseen during training phase). The best architecture among the tested ones was then found to consist of 2 hidden layers composed of 893 neurons each (see Fig. 1).

In supervised learning, the data must be labeled. However, the optimal labels are not well-defined in our case. From the Bayesian estimation perspective, this would require having access to the true distribution (i.e., the standard deviation in particular, assuming a Gaussian distribution of the measurements errors), while only a single sample of this distribution is available. Indeed, having more precise information about the underlying distribution would require collecting multiple measurements from the same receiver's position with also the same SV positions, which is not feasible. When dealing with a single sample/observation, the most accurate estimate of the standard deviation is the absolute value of the error calculated specifically for that measurement. This approach is further reinforced by empirical evidence, by utilizing the weights as:

$$\omega^i = 1/(\rho^i - h(\mathbf{X}_{true}))^2, \quad (9)$$

where the \mathbf{X}_{true} stands for the ground-truth position collected from the reference system. Utilizing this weighting method has provided very good results as shown in Fig. 7 and 8, thus these weights were used as the data labels.

As a first example, we have analyzed a vehicular setup of 40 minutes, comprising urban, sub-urban and back-country environments using the ZED-F9P receiver chip. For this test, the horizontal error for the SOTA single-epoch algorithm is only 2.18 m, which can be qualified as good when compared to the accuracy of the 2.03 m solution provided by the receiver benefiting from a filtered mode. Our approach offers a

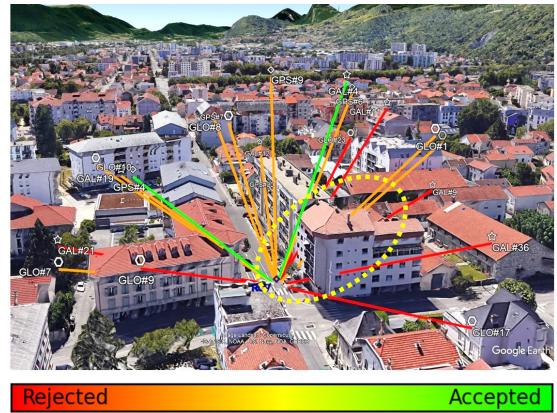


Fig. 4. Conceptual illustration of satellite measurements weighting with the proposed approach.

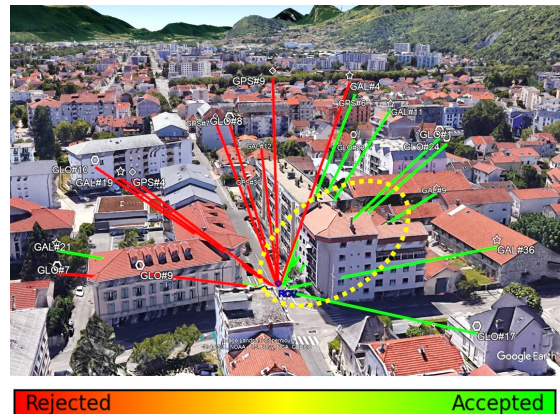


Fig. 5. Conceptual illustration of satellite measurements weighting with the SOTA approach [18], for the same epoch as that of Fig. 4.

significant performance improvement (of 35%) with only 1.41 m of error.

To provide a better understanding of the possible benefits of our approach, we focus next on a specific epoch in a sub-urban environment, where the difference with SOTA is quite significant. For qualitative benchmark purposes, Fig. 4 and 5 illustrate the satellite links in this setup and how the satellites were treated by the two approaches, where the color bar indicates the degree (between accepted or rejected) of the weights used for positioning. As it can be seen, SVs GAL#36, GAL#9, GLO#24, GLO#1, etc. are clearly in NLOS conditions. These SVs were not rejected by the SOTA approach (see Fig. 5), while they were either rejected or weighted by our approach (see Fig. 4). Furthermore, other SVs in LOS conditions such as GPS#9, GPS#7, GLO#8, GAL#12, etc. were completely rejected by the SOTA approach, while being efficiently weighted by our approach.

Fig. 6 represents another comparison of our approach with SOTA, focusing on a specific portion of one navigation session in a GNSS-challenging environment (urban canyon). The deviation of the localized position with our approach from the reference one is much less than that of the SOTA approach. In this case, several strongly biased SVs in NLOS conditions, such as GPS#12, GPS#32, and GLO#9, were used by the SOTA approach to calculate a position estimation,

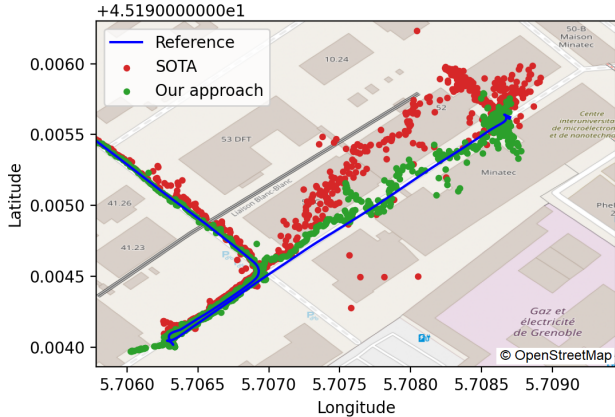


Fig. 6. Example of positioning traces obtained in a field navigation session (urban canyon) with the proposed approach (green dots), the one in [18] from recent state-of-the-art (red dots), and the ground-truth reference system (blue solid line).

whereas in our approach the same SVs have been excluded from the solution by assigning them very low weights (i.e., $\omega^{GPS\#12} = 0.0016$, $\omega^{GPS\#32} = 0.0006$, $\omega^{GLO\#9} = 0.002$), hence resulting in a much better accuracy of 2.06 m typically. In other words, our approach seems more robust and suited to highly challenging environments, by mitigating the influence of strongly biased measurements through adequate weighting.

Finally, Fig. 7 and 8 show the empirical cumulative density function (CDF) of horizontal and vertical positioning errors obtained with four different weighting strategies over all navigation sessions from ZED-F9P receiver (386,000 epochs): the first one, referred to as “Ground-truth Weights”, utilizes weights as in (9) with the ground-truth position, before applying WLS positioning. The second method, named “Feature Matrix”, exploits the overall feature matrix comprising the two sub-matrices (i.e., the “Residual Matrix” concatenated with the additional per-link features) as an input to the NN to predict link-wise quality factors which are then used to compute weights as in (4) for WLS positioning. The third method, named “Residual Matrix”, uses only the residual matrix (joint features) as an input to the proposed algorithm. Finally, in the fourth “SOTA” method, the state-of-the-art solution from [18] (See Section II-C) is used for positioning.

We thus observe a significant improvement in terms of both horizontal and vertical errors of the deep learning approaches compared to the state-of-the-art solution. On the one hand, “Feature Matrix” exhibits a performance gain with respect to the SOTA approach of 1 m (resp. 1.47 m) in terms of horizontal error at 68% (resp. 95%) of the CDF. As for the vertical error, we also observe an improvement of 1.2 m (resp. 1.75 m) at 68% (resp. 95%) of the CDF. On the other hand, the “Residual Matrix” approach shows a performance gain compared to the SOTA approach of 0.61 m (resp. 1.38 m) in terms of horizontal error at 68% (resp. 95%) of the CDF. As for the vertical error, we also observe an improvement of 0.66 m (resp. 1.43 m) at 68% (resp. 95%) of the CDF.

It is worth highlighting that the additional per-link features concatenated with the residuals have a significant and positive

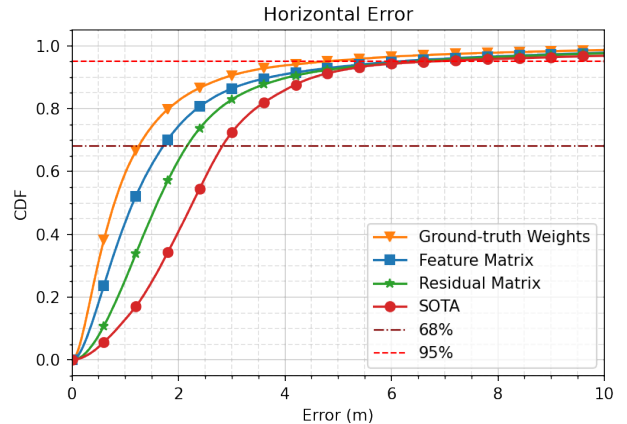


Fig. 7. Empirical CDF of horizontal error for various measurements weighting/selection strategies (incl. [18]) on real field data (over all navigation sessions from ZED-F9P receiver).

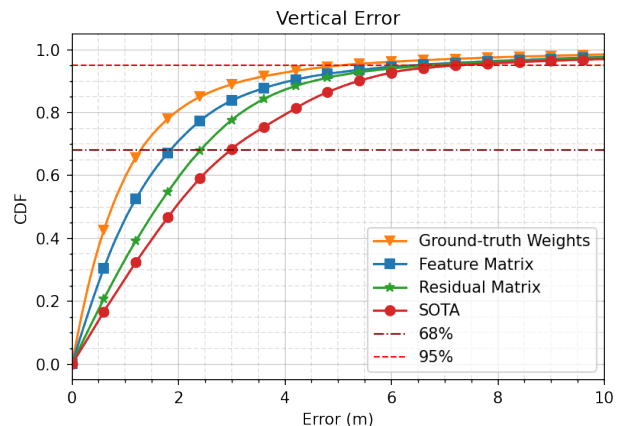


Fig. 8. Empirical CDF of horizontal error for various measurements weighting/selection strategies (incl. [18]) on real field data (over all navigation sessions from ZED-F9P receiver).

impact on the positioning accuracy. The superiority of the proposed approaches on the tested data illustrates their relative robustness in various operating conditions.

V. CONCLUSIONS

In this paper, we introduced a novel approach for SV measurement weighting in single-epoch GNSS positioning by exploiting a combination of joint features (i.e., conditional pseudorange residuals) and per-link features (i.e., C/N_0 and its empirical statistics, SV elevation angle, carrier phase lock time). Our approach relies on a LSTM NN in predicting several quality factors to weight the contributions of different measurement into the calculation of a position. Our results on real data obtained from field experiments demonstrated the robust performance of the proposed solution in challenging environments, while outperforming a recent SOTA approach. This solution is particularly promising into IoT applications (remote processing), where accurate single-epoch positioning is essential, whether in real-time or offline.

ACKNOWLEDGEMENT

The work included in this paper has been partly supported by the “France 2030” investment program through the project 5G-OPERA.

REFERENCES

- [1] M. S. Grewal, L. Weill, and A. P. Andrews, *Global positioning systems, inertial navigation and Integration*. Hoboken, NJ: Wiley, 2007.
- [2] *LR1110 Low Power Wi-Fi/GNSS Scanner + Lora Transceiver*, Semtech, 12 2021, rev. 1.3.
- [3] H. Hartinger and F. K. Brunner, "Variances of gps phase observations: The sigma- ϵ model," *GPS Solutions*, vol. 2, no. 4, pp. 35–43, 1999.
- [4] F. K. Brunner, H. Hartinger, and L. Troyer, "Gps signal diffraction modelling: the stochastic sigma- δ model," *Journal of Geodesy*, vol. 73, pp. 259–267, 1999.
- [5] N. Zhu, J. Marais, D. Bétaille, and M. Berbineau, "Evaluation and comparison of gnss navigation algorithms including fde for urban transport applications," *Proceedings of the 2017 International Technical Meeting of The Institute of Navigation*, pp. 51–69, 2017.
- [6] G. Castaldo, A. Angrisano, S. Gaglione, and S. Troisi, "P-ransac: An integrity monitoring approach for gnss signal degraded scenario," *International Journal of Navigation and Observation*, vol. 2014, 2014.
- [7] M. A. Akram, P. Liu, Y. W. ID, and J. Qian, "Gnss positioning accuracy enhancement based on robust statistical mm estimation theory for ground vehicles in challenging environments," *Applied Sciences*, vol. 8, no. 6, 2018.
- [8] J. Zhao, C. Xu, Y. Jian, and P. Zhang, "A modified range consensus algorithm based on ga for receiver autonomous integrity monitoring," *Mathematical Problems in Engineering*, vol. 2020, 2020.
- [9] R. J. Rossi, *Mathematical Statistics: An Introduction to Likelihood Based Inference*. Hoboken, NJ: Wiley, 2018.
- [10] J. J. Moré, "The levenberg-marquardt algorithm: Implementation and theory," in *Numerical Analysis*, G. A. Watson, Ed. Berlin, Heidelberg: Springer Berlin Heidelberg, 1978, pp. 105–116.
- [11] P. Groves, *Principles of GNSS, Inertial, and Multisensor Integrated Navigation Systems*. Boston: Artech House, 2013.
- [12] N. Zhu, D. Bétaille, J. Marais, and M. Berbineau, "Extended kalman filter (ekf) innovation-based integrity monitoring scheme with c / n0 weighting," in *2018 IEEE 4th International Forum on Research and Technology for Society and Industry (RTSI)*, 2018, pp. 1–6.
- [13] N. Knight and J. Wang, "A comparison of outlier detection procedures and robust estimation methods in gps positioning," *Journal of Navigation*, vol. 62, pp. 699 – 709, 10 2009.
- [14] H. Kuusniemi, A. Wieser, G. Lachapelle, and J. Takala, "User-level reliability monitoring in urban personal satellite-navigation," *IEEE Transactions on Aerospace and Electronic Systems*, vol. 43, no. 4, pp. 1305–1318, 2007.
- [15] Y. Zhai, M. Joerger, and B. Pervan, "Fault exclusion in multiconstellation global navigation satellite systems," *Journal of Navigation*, vol. 71, no. 6, pp. 1281–1298, 2018.
- [16] M. Joerger, F. Chan, and B. Pervan, "Solution separation versus residual-based raim," *Journal of the Institute of Navigation*, vol. 61, no. 4, pp. 273–291, 2014.
- [17] A. Angrisano, C. Gioia, S. Gaglione, and G. Core, "Gnss reliability testing in signal-degraded scenario," *International Journal of Navigation and Observation*, vol. 2013, no. 870365, 2013.
- [18] C. Combettes and C. Villien, "Ekf based on two fde schemes for gnss vehicle navigation," in *2021 IEEE 93rd Vehicular Technology Conference (VTC2021-Spring)*, 2021, pp. 1–6.
- [19] A. Pirsivash, "Gnss signal and measurement quality monitoring for multipath detection and mitigation," 08 2019.
- [20] K. Huang, A. Hussain, Q.-F. Wang, and R. Zhang, Eds., *Deep Learning: Fundamentals, Theory and Applications*. Springer Cham, 2019.
- [21] A. Graves and J. Schmidhuber, "Offline handwriting recognition with multidimensional recurrent neural networks," *Proceedings of the 20th International Conference on Neural Information Processing Systems*, p. 577–584, 2007.